INL/CON-06-12026
PREPRINT

One-Dimensional Analysis of Thermal Stratification in AHTR and SFR Coolant Pools

NURETH-12

Haihua Zhao
Per F. Peterson

October 2007

The INL is a
U.S. Department of Energy
National Laboratory
operated by
Battelle Energy Alliance

ONE-DIMENSIONAL ANALYSIS OF THERMAL STRATIFICATION IN AHTR AND SFR COOLANT POOLS

Haihua Zhao *
Idaho National Laboratory
Idaho Falls, ID 83415-3890, USA
Haihua.Zhao@inl.gov

Per F. Peterson
Nuclear Engineering Department
University of California
Berkeley, CA 94720, USA
peterson@nuc.berkeley.edu

ABSTRACT

Thermal stratification phenomena are very common in pool type reactor systems, such as the liquid-salt cooled Advanced High Temperature Reactor (AHTR) and liquid-metal cooled fast reactor systems. It is important to accurately predict the temperature and density distributions both for design optimization and accident analysis. Current reactor system analysis codes only provide lumped-volume based models that can give very approximate results and can only handle simple cases with one mixing source. While CFD methods can be used to analyze simple configurations, these methods require very fine grid resolution to resolve thin substructures such as jets and wall boundaries, yet such fine grid resolution is difficult or impossible to provide for studying the reactor response to transients due to computational expense. Therefore, new methods are needed to support design optimization and safety analysis of Generation IV pool type reactor systems.

Previous scaling has shown that stratified mixing processes in large stably stratified enclosures can be described using one-dimensional differential equations, with the vertical transport by free and wall jets modeled using standard integral techniques. This allows very large reductions in computational effort compared to three-dimensional numerical modeling of turbulent mixing in large enclosures. The BMIX++ (Berkeley mechanistic MIXing code in C++) code was originally developed at UC Berkeley to implement such ideas. By including liquid salt properties, BMIX++ code is extended to analyze liquid salt pool systems in the current AHTR baseline design, to provide an example of its application. Similar analysis is possible for liquid-metal cooled reactors.

KEYWORDS
Thermal stratification, AHTR, SFR, One-dimensional

* Corresponding author. Phone: +1 (208) 526-2679, Fax: +1 (208) 526-0528

1. INTRODUCTION

Thermal stratification phenomena are very common in pool type reactor systems, such as the liquid-salt cooled Advanced High Temperature Reactor (AHTR) [1, 2] and liquid-metal cooled fast reactor systems such as the Sodium Fast Reactor (SFR) [3]. It is important to accurately predict the temperature and density distributions both for design optimization and accident analysis. Current major reactor system analysis codes such as RELAP5 (for LWR's, and recently extended to analyze high temperature reactors) [4], TRAC (for LWR's) [5], and SASSYS (for liquid metal fast reactors) [6] only provide lumped-volume based models which can only give very approximate results and can only handle simple cases with one mixing source at best. While 2-D or 3-D CFD methods can be used to analyze simple configurations, these methods require very fine grid resolution to resolve thin substructures such as jets and wall boundaries, yet such fine grid resolution is difficult or impossible to provide for studying the reactor response to transients due to computational expense. Therefore, new methods are needed to support design optimization and safety analysis of Generation IV pool type reactor systems.

Previous scaling has shown that stratified mixing processes in large stably stratified enclosures can be described using one-dimensional differential equations, with the vertical transport by free and wall jets modeled using standard integral techniques[7]. This allows very large reductions in computational effort compared to three-dimensional numerical modeling of turbulent mixing in large enclosures. The BMIX++ (Berkeley mechanistic MIXing code in C++) code was originally developed at UC Berkeley to implement such ideas [8, 9, and 10]. This code solves transient mixing and heat transfer problems in stably stratified enclosures. The code uses a Lagrangian approach to solve 1-D transient governing equations for the ambient fluid and uses analytical or 1-D integral models to compute substructures such as circular/line buoyant jets, wall boundary flows/wall jets, etc. 1-D solid conduction model is also included in the code.

The basic requirements for using the BMIX++ code are 1-D stable stratification or nearly stable stratification. When such conditions are met, various problems with different combinations can be solved by the BMIX++ code, such as: multi-component fluid, variable enclosure cross section area in vertical direction, multi-enclosures, and multiple jets, plumes, and sinks in one enclosure. Available substructure models in the current version include curved free circular buoyant jets, vertical line buoyant jets, isothermal wall jets, and boundary wall conductions. The problems that can be solved with the code vary from the classic filling box model, such as the case studied by Baines and Turner [11], the experiments of stratification in a cylinder generated by an internal heat source by Fox et al. [12], complex multi-substructures mixing experiments such as the large containment mixing experiments in UC Berkeley [9, 10], even the complex long-term containment accident analysis in advanced light water reactors when steam-water jet and condensation models are available [13]. If a radiation model is added to the code, building fires can be analyzed.

By including liquid salt properties, BMIX++ code is extended to analyze liquid salt pool systems in the current AHTR design, to provide an example of its application. Similar analysis is possible for liquid-metal cooled reactors. The current AHTR baseline design [2] uses a large buffer salt tank to provide more thermal inertial and safety margin. Reactor vessel, intermediate heat exchangers (IHX), pool reactor auxiliary cooling system (PRACS) heat exchangers (PHX),

and direct reactor auxiliary cooling system (DRACS) heat exchangers (DHX) are all immersed in the buffer salt pool. These structures provide driving sources for vertical mixing and thermal stratification. Predication of the temperature distribution within the buffer salt tank directly affects the major safety systems design, such as the PHX and DHX, safety analysis results, and structure thermal stresses analysis. The BMIX++ code is used to predict mixing and thermal stratification in this pool system. This example shows the potential of 1-D analysis methods and BMIX++ to be included in system analysis codes for pool type of Gen-IV reactor systems.

2. SUMMARY OF MAJOR MODELS

2.1. 1-D Governing Equations for Mixing in Stably Stratified Enclosure

Previous scaling analysis [7] has shown that the ambient fluid between jets tends to organize into either a homogeneously mixed condition or a vertically stratified condition that can be described by a one-dimensional temperature and concentration distribution. Furthermore, the transition between the well-mixed and stratified conditions can be predicted. Thus, we can describe stratified mixing processes in large, complex enclosures using one-dimensional differential equations, with transport in free and wall jets modeled using integral models. The detailed geometry of the enclosure becomes unimportant, and only the horizontal cross-sectional area and perimeter must be specified as a function of elevation. This allows very large reductions in computational effort compared to three-dimensional numerical modeling of turbulent mixing in large enclosures. Large enclosures mixed by buoyant plumes and wall jets can normally be expected to stratify. For the stratified enclosure, the governing equations for ambient fluid can be derived and written in the following compact form,

$$A(z)\frac{\partial \mathbf{G}}{\partial t}+\frac{\partial \mathbf{F}}{\partial z}=\mathbf{S} \tag{1}$$

where A(z) is the horizontal cross sectional area of the volume at elevation z, and **G**, **F**, and **S** are the vectors of conserved quantities, fluxes, and source terms respectively,

$$\mathbf{G}=\begin{pmatrix}\rho\\0\\\rho h\\\rho\chi_1\\\vdots\\\rho\chi_{ns-1}\end{pmatrix}\quad \mathbf{F}=\begin{pmatrix}\rho Q_{sf}\\P\\\rho h Q_{sf}-Ak\dfrac{\partial T_{sf}}{\partial z}\\\rho\chi_1 Q_{sf}-\rho AD\dfrac{\partial \chi_1}{\partial z}\\\vdots\\\rho\chi_{ns-1}Q_{sf}-\rho AD\dfrac{\partial \chi_{ns-1}}{\partial z}\end{pmatrix}\quad \mathbf{S}=\begin{pmatrix}-\sum_{k=1}^{n}(\rho Q')_k+\rho S'-\rho\hat{S}'\\-\rho g\\-\sum_{k=1}^{n}(\rho hQ')_k+\rho S'_h-\rho\hat{S}'_h\\-\sum_{k=1}^{n}(\rho\chi_1 Q')_k+\rho\chi_1 S'-\rho\chi_1\hat{S}'\\\vdots\\-\sum_{k=1}^{n}(\rho\chi_{ns-1}Q')_k+\rho\chi_{ns-1}S'-\rho\chi_{ns-1}\hat{S}'\end{pmatrix} \tag{2}$$

Where ρ is the mixture density, h enthalpy, χ mass fraction, Q volume flow rate, P pressure, k thermal conductivity, T temperature, D mass diffusion coefficient, Q' jet volumetric entrainment rate per unit length, n the total number of jets, S' and $\hat{S}'$ volumetric source and sink per unit length, S'_h and $\hat{S}'_h$ volumetric energy source and sink per unit length, and ns and sf are subscripts denoting the number of species and stratified ambient fluid respectively.

2.2.Lagrangian Method for the Ambient Fluid

The numerical methods traditionally used to solve the conservation equations have great difficulty in preserving strong gradients in hyperbolically dominated flows. The traditional discretization procedures inherently introduce artificial diffusion terms. Typically, these extra diffusion terms put severe limitations on the maximum size of the computational control volume for the computed solution to be reasonably accurate. Therefore, the BMIX++ code uses an alternative to the traditional numerical methods to:

- eliminate "false diffusion" from the discretized equations;
- give physically acceptable solutions even for coarse computational grids;
- have favorable stability requirements, i.e. a very lax stability requirement;
- and require low computational cost.

A Lagrangian approach was adopted to eliminate numerical diffusion [8]. The Lagrangian formulation tracks the position of constant mass fluid "layers". In practice, the enclosure is divided into a user-specified number of horizontal control volumes. The conservation equations, without the diffusion terms, are then used to calculate the new positions, compositions and enthalpies of the control volumes for each time step. Next, the composition and energy are corrected according to the diffusion terms in the conservation equations.

The discrete Lagrangian conservation equations (mass, species mass, and energy) are given below [8]:

$$V_k^{j+1} - V_k^j = \Delta t\left\{-\sum_{l=1}^{L} Q_{k,l}^j + A_{k+1}^j \sum_{i=1}^{I} \dot{V}''^j_{i,k+1} - A_k^j \sum_{i=1}^{I} \dot{V}''^j_{i,k} + S_k^j - \hat{S}_k^j\right\} \tag{3}$$

$$\overline{\chi}_{i,k}^{j+1} V_k^{j+1} - \overline{\chi}_{i,k}^j V_k^j = \Delta t\left\{-\overline{\chi}_{i,k}^j \sum_{l=1}^{L} Q_{k,l}^j + A_{k+1}^j \dot{V}''^j_{i,k+1} - A_k^j \dot{V}''^j_{i,k} + S_{i,k}^j - \hat{S}_{i,k}^j\right\} \quad \text{for i} = \{1,2,...,(\text{I}-1)\} \tag{4}$$

$$\overline{h}_{k,mix}^{j+1} V_k^{j+1} - \overline{h}_{k,mix}^j V_k^j = \Delta t\left\{-\sum_{i=1}^{I} \overline{h}_{i,k}^j \overline{\chi}_{i,k}^j \sum_{l=1}^{L} Q_{k,l}^j + A_{k+1}^j \sum_{i=1}^{I} \overline{h}_{i,a_{i,k+1}}^j \dot{V}''^j_{i,k+1} - A_k^j \sum_{i=1}^{I} \overline{h}_{i,a_{i,k}}^j \dot{V}''^j_{i,k} + \frac{1}{\overline{\rho}}\left(A_{k+1}^j q''^j_{k+1} - A_k^j q''^j_k + S_{h,k}^j - \hat{S}_{h,k}^j\right)\right\} \tag{5}$$

where the superscripts j and $j+1$ indicate the time level ($t = j\Delta t$), the subscript 'i' corresponds to the *ith* component of the fluid, subscript 'k' indicates the *kth* control volume, and subscript 'l' the *lth* buoyant jet. V is volume [m^3], Δt time step length [s], L number of buoyant jets present in the enclosure [−], $Q_{k,l}$ volumetric flow rate entrained by buoyant jet l within control volume k [m^3/s], A horizontal cross-sectional area [m^2], $\dot{V}''$ volumetric flow rate per unit area due to molecular diffusion [m^3/(m^2.s)], S and $\hat{S}$ volume source and sink, respectively [m^3/s], $\overline{\chi}$ volume averaged mass fraction [−], $\overline{h}_{mix}$ volume averaged mixture enthalpy [J/kg], $\overline{\rho}$ volume averaged total density [kg/m^3], q'' heat flux due to heat diffusion [W/m^2], S_h and $\hat{S}_h$ source and sink respectively of energy per unit time [W], Δz step length in the z-direction [m]. The subscript $a_{i,k}$

used in the energy equation Eq. (5), accounts for the direction of the diffusive mass flux and is defined by

$$a_{i,k} \equiv \begin{cases} k, & \left.\dfrac{\partial \chi_i}{\partial z}\right|_{z=z_k} > 0 \\ k-1, & \left.\dfrac{\partial \chi_i}{\partial z}\right|_{z=z_k} \le 0 \end{cases} \tag{6}$$

The stability for this set of difference equations is guaranteed provided that negative control volumes are not permitted to occur at any time (the non-negative requirement). Contrast this stability requirement with the Courant-Friedrichs-Levy (CFL) stability criterion encountered for standard finite difference methods. The CFL-condition bounds the ratio $\Delta t/\Delta z$, which means that Δt_{max} is determined by the smallest spatial computational cell (Δz) in the computational domain and increasing spatial resolution (smaller Δz) requires a smaller time step length. For the Lagrangian method, Δz can be chosen independently of Δt. The stability criterion is so lax that in practice the maximum tolerable time step length is limited by accuracy, i.e., the size of the truncation error limits the time step length.

Choosing a Lagrangian method also has its costs mostly due to a more complicated implementation, because the position of every control volume must be tracked. In general, having a moving computational grid implies more bookkeeping and makes the implementation of virtually all aspects of the code less automatic compared to a standard finite difference method (FDM). One example of the complication is the necessity of grid management. At each time step, new control volumes are created at elevations where fluid injection occurs, and so both the number of control volumes and the computational cost increase linearly with time. The size of the CV added varies linearly with time step length since the total entrained volumetric flow rate is given and is time independent. Therefore, the fineness of the computational grid is proportional to the time step length.

The basic idea of grid management is merging of smaller CVs (control volumes) with their neighbors according to some criteria while keeping the necessary precision. Two types of grid management are provided in the BMIX++ code. The first scheme is based on the relative minimal volume of CVs. The second scheme is based on the relative minimal density difference between two neighboring CVs. The volume-based grid management is necessary for the calculation with a large number of time steps. For example, if for each time step half of the fluid in a volume is entrained by a jet and the machine numerical precision is assumed about 10^{-16}, then the volume of the CV will reach the machine numerical precision after n time steps:

$(1/2)^n = 10^{-16}$, $\quad n \cong 53$.

Therefore, after 53 time steps the volume of the CV will be in the order of machine numerical precision and the code is doomed to crash. The volume-based grid management algorithm searches all the CVs and finds out those CVs whose volumes are less than the minimal value given by users; and then merges those CVs with their smaller neighbor CVs. The second scheme is useful to provide higher resolution in regions where temperature or density gradients are steep while keeping optimal efficiency. The temperature/density-based grid management algorithm searches all the CVs and finds the pairs of neighboring CVs whose temperature differences are less than the value given by users. Using this algorithm, the temperature profile can be well

preserved. Finer grids are automatically applied in the region where the temperature gradient is larger; coarser grids emerge in the regions where the temperature gradient is smaller. Volume-based grid management and temperature-based grid management can be used simultaneously to improve the efficiency of computation.

2.3 Models for Plumes and Jets

In this paper a jet should be understood as a generic concept of any steady continuous flow structure in an ambient volume with a dominant flow direction and a length scale much less than the ambient volume's scale. For example, a plume (due to a heat source), a pure jet (due to an initial momentum source), a buoyant jet (due to both buoyancy and momentum), a wall jet along a wall surface, or a wall boundary flow are all taken as jets. All these jet concepts have one common character: the jet entrains fluid from the ambient volume and finally discharges into the ambient volume. In most engineering problems, jets are turbulent flow. In the BMIX++ code, all the jets are assumed turbulent except those specifically noted as being laminar. This section only describes two physical models for circular buoyant jets due to the page limit.

2.3.1 Integral model for vertical buoyant jets

The concept of a vertical buoyant jet can include vertical pure jets, pure plumes, vertical buoyant jets or forced plumes. Only steady jets are considered. Morton [14] used the fundamental assumption by G. I. Taylor that the entrainment velocity is a fraction of the buoyant jet centerline velocity. The Morton plume model can treat vertical buoyant jets generated by both thermal expansion and vertically injected fluid (the direction of injection has to match the sign of the buoyancy). The plume is assumed to have Gaussian profiles of mean vertical velocity and mean buoyancy. If ambient is of uniform density, the centerline properties of the plume can be expressed in terms of powers of z and the buoyancy flux:

$$b = \frac{6}{5}\alpha z, \tag{7}$$

$$U = \frac{5}{6\alpha}\left(\frac{18}{5\pi}\alpha B\right)^{1/3} z^{-1/3}, \tag{8}$$

$$g' = \frac{5}{3\pi}\left(\frac{5\pi}{18}\right)^{\frac{1}{3}} \alpha^{-\frac{4}{3}} B^{\frac{2}{3}} z^{-\frac{5}{3}}, \tag{9}$$

where b is jet width scale [m], z the elevation from the source and the entrainment constant [m], α [-], is defined as the fraction of entrainment (inward) velocity to the centerline velocity U [m/s]. In mathematical terms we can write

$$v_r = -\alpha|U|, \tag{10}$$

where v_r [m/s] is the radial velocity using a cylindrical polar coordinate system (the absolute value of U allows for both upward and downward directed buoyant jets). The entrainment constant, α, is empirically determined. B is the buoyancy flux [m^4/s^3], which is defined for a heat source by

$$B = \frac{g\beta\dot{q}}{\rho_{amb} c_p}, \tag{11}$$

where g is gravitational acceleration [m/s^2], β constant of thermal expansion [1/K], $\dot{q}$ heating rate [W], ρ_{amb} density of the ambient fluid [kg/m^3], and c_p specific heat at constant pressure [J/(kg-K)]. And for injected fluid by

$$B = gQ_{in}\frac{\rho_{amb} - \rho_{in}}{\rho_{amb}}, \tag{12}$$

Where Q_{in} is inlet volume flow rate of jet [m^3/s] and ρ_{in} inlet jet fluid density [kg/m^3]. Formally, we may write the volumetric flow rate of the buoyant jet, Q_p [m^3 /s], as

$$Q_p \equiv 2\pi \int_0^\infty \bar{u} r dr = \pi U b^2 \tag{13}$$

Combining Eqs. (7) and (8) reveals the following expression for the buoyant jet volumetric flow

$$Q_p = \frac{6\pi}{5}\alpha^{4/3}\left(\frac{18}{5\pi}\right)^{1/3} B^{1/3} z^{5/3}, \tag{14}$$

Another definition of the entrainment constant often occurs in the plume literature. Here the volumetric flow rate carried by a buoyant jet, Q_p [m^3/s], is defined as [7]

$$Q_p = k_\mu B^{1/3} z^{5/3}, \tag{15}$$

giving a volumetric entrainment rate per unit length, Q'_{entr} [m^2/s],

$$Q'_{entr} \equiv \frac{d}{dz} Q_p = \frac{5}{3} k_\mu B^{1/3} z^{2/3}, \tag{16}$$

where k_μ [-] is Taylor's entrainment constant. In the BMIX++, k_μ=*0.15* is set as default value and α=*0.086*.

2.3.2 Schatzmann's model for circular free curved buoyant jets

Among numerous integral models for circular buoyant jets, the model presented by Schatzmann [15, 16] appears to be the most mathematically rigorous and the most physically complete [17]. Therefore, this model was selected to simulate a generic steady circular buoyant jet. Schatzmann's model is for the prediction of spreading and rising of circular buoyant jets discharged at any angle into a stratified, flowing ambient fluid. The model is based on the differential equations for the conservation of mass, momentum, concentration and thermal energy. These equations are transformed by vector operations in a streamwise coordinate system and integrated in the angular and radial directions using symmetry and similarity assumptions. The common Boussinesq approximation was not used, because the density difference between the jet and the ambient flow could be large. The Gaussian profile is used. For velocity and density, the profiles are:

$$u(s,r)/u^*(s) = e^{-r^2/b(s)^2}, \tag{17}$$

$$(\rho(s,r)-\rho_a)/\rho^*(s)=e^{-r^2/(\lambda b(s))^2}, \tag{18}$$

where s is the streamwise coordinate, distance along the jet axis; r the radial coordinate, distance from jet centerline; $u(s, r)$ the velocity at (s, r); $u^*(s)$ the jet centerline velocity; b the jet width scale; ρ density; subscript a indicates ambient; ρ^* is the centerline excess density over ambient; λ is the ratio of spreading of the density and velocity profiles. Figure 1 shows the coordinate system.

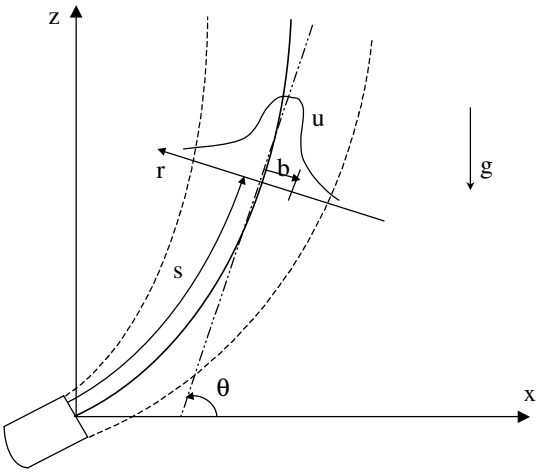

Figure 1 Coordinate System Used For Buoyant Jet Analysis.

The original Schatzmann's model was simplified for the quiescent ambient considered in the BMIX++ code. The following are the simplified governing equations:
Continuity equation:

$$\frac{d}{ds}\left[\left(\rho_a+\frac{\lambda^2}{\lambda^2+1}\rho^*\right)u^*b^2\right]=2\rho_a b u^*\varepsilon, \tag{19}$$

s direction momentum equation:

$$\frac{d}{ds}\left[\left(\frac{1}{2}\rho_a+\frac{\lambda^2}{2\lambda^2+1}\rho^*\right)u^{*2}b^2\right]=-\lambda^2 b^2\rho^* g\sin\theta, \tag{20}$$

θ direction momentum equation:

$$\frac{d\theta}{ds}=-\frac{\lambda^2 g\rho^*\cos\theta}{u^{*2}\left(\frac{1}{2}\rho_a+\frac{\lambda^2}{2\lambda^2+1}\rho^*\right)}, \tag{21}$$

Energy conservation equation:

$$\frac{d}{ds}\left[\left(\frac{\lambda^2}{\lambda^2+1}\rho_a+\frac{\lambda^2}{\lambda^2+2}\rho^*\right)b^2u^*T^*\right]=-\left(\frac{dT_a}{ds}\right)\left(b^2u^*\right)\left(\rho_a+\frac{\lambda^2}{\lambda^2+1}\rho^*\right), \tag{22}$$

Trajectory equation:

$$\frac{dx}{ds} = \cos\theta\,, \tag{23}$$

$$\frac{dz}{ds} = \sin\theta\,, \tag{24}$$

Mass concentration of component i equation:

$$\frac{d}{ds}\left[\left(\frac{\lambda^2}{\lambda^2+1}\rho_a + \frac{\lambda^2}{\lambda^2+2}\rho^*\right)b^2u^*c_i^*\right] = -\left(\frac{dc_{ia}}{ds}\right)\left(b^2u^*\right)\left(\rho_a + \frac{\lambda^2}{\lambda^2+1}\rho^*\right)\text{, for i=1,...I-1} \tag{25}$$

Where superscript * denotes the jet excess value at the centerline over the ambient value; subscript a indicates the ambient value; θ is the angle with the horizontal; c_i^* is the mass concentration of component i, [kg_i/kg_{mix}]; I is the number of components; if I is 1, then mass concentration is not needed. Note that $\sum_{i=1}^{I} c_i = 1$, so only (I-1) mass concentration equations are needed.

Centerline velocity u^*, jet nominal width b, centerline temperature excess T^*, angle with the horizontal θ, horizontal coordinate x, vertical coordinate z, and mass concentration of component i c_i (if I>1) are variables need to be solved, respectively. The equation group is completed by the state equation $\rho^* = \rho^*\left(p, T^*, c_1^*, \cdots, c_{I-1}^*, T_a, c_{a1}, \cdots c_{a(I-1)}\right)$ and an entrainment model. The entrainment assumption by Teixeira and Miranda [18] is used to complete the equations. This entrainment model is based on a first-order turbulence closure, which only requires two adjustable constants while Schatzmann's original entrainment model requires four constants. The entrainment model by Teixeira and Mirranda is:

$$\varepsilon = 3\beta - \frac{(2\lambda^2-1)\lambda^2}{\lambda^2+1}\frac{\sin\theta}{Fr^2}\,, \tag{26}$$

where the square of the local densimetric Froude number is defined as

$$Fr^2 = \frac{u^{*2}}{gb\rho^*/\rho_a}\,, \tag{27}$$

The constants in Eq. (26) are $\beta = 0.019$, $\lambda = 1.16$.

For buoyant jets with an initial flow rate, the initial conditions have been derived from the results of several experiments [17]. The initial point for the model is set at the end of the flow development region, a distance

$$s_0 = n_d D\,, \tag{28}$$

from the source, where n_d is a constant between 0 to 6.2. For a jet injected from a fully developed circular pipe flow, 6.2 is used. D is the diameter of the source. At this point, the jet trajectory angle is given empirically as

$$\theta_0 = \theta_j , \tag{29}$$

where j is the jet source condition. The initial values of the remaining jet variables are given by

$$u_0^* = u_j^* , \tag{30}$$

$$b_0 = D/\sqrt{2} , \tag{31}$$

$$T_0^* = T_j^* \frac{\lambda^2 + 1}{2\lambda^2} , \tag{32}$$

$$c_{i0}^* = c_{ij}^* \frac{\lambda^2 + 1}{2\lambda^2} , \quad \text{i=1, ..., I-1} \tag{33}$$

Eq. (30) is based on the notion of a potential core, while Eqs. (31)-(33) are developed by balancing fluxes through the flow development region without any entrainment of the ambient fluid.

For a pure plume, initial values for centerline velocity u^*, jet nominal width b, centerline temperature excess T^*, and mass concentration of component i c_i (if I>1) are obtained from the pure plume model by Morton [14], the virtual source concept [19], and the strong-plume extension of the weak-plume model [20]. For the case of a pure plume, the distance z_v from the source to the virtual origin is related to the source radius, R_s, by

$$z_v = \frac{5}{6\alpha_T} R_s , \tag{34}$$

where α_T=*0.12* is the entrainment coefficient for the top hat profile. Morton's extension of the weak-plume theory based on the work of Ricou and Spalding led to the result that g' in Eq. (9) should be replaced by $g\frac{\rho_\infty - \rho_0}{\rho_0} \left(= g\Delta T / T_\infty\right)$ and the additional factor $\left(\rho_\infty / \rho_0\right)^{1/2}$ should be introduced on the right-hand side of the Eq. (8). Therefore, the initial values of the remaining plume variables are given by

$$b_0 = \frac{6}{5}\left(\frac{\rho_\infty}{\rho_0}\right)^{\frac{1}{2}} \alpha z_v , \tag{35}$$

$$u_0^* = \frac{5}{6\alpha}\left(\frac{18}{5\pi}\alpha B\right)^{1/3} z_v^{-1/3} , \tag{36}$$

$$T_0^* = \frac{T_\infty}{g}\frac{5}{3\pi}\left(\frac{5\pi}{18}\right)^{\frac{1}{3}} \alpha^{-\frac{4}{3}} B^{\frac{2}{3}} z_v^{-\frac{5}{3}} , \tag{37}$$

$$c_{i0}^* = 0 , \quad \text{i=1, ..., I-1} \tag{38}$$

The equation system is numerically solved by Runge-Kutta-Fehlberg method [21]. The initial values according to Eqs. (29) to (33) are applied for the buoyant jet, and initial values according to Eqs. (35) to (38) are applied for the pure plume. The Runge-Kutta method is one of the most commonly used algorithms for the solution of an IVP (Initial Value Problem) of ODEs (Ordinary Differential Equations).There are several versions of the RK (Runge-Kutta) methods, depending on the desired reduction of the truncation error. The fourth order version is the most popular one. An improvement over RK is RKF (Runge-Kutta-Fehlberg method), which has the advantage of automatically adjusting the step length to meet any given error tolerance. The RKF algorithm is selected to solve jet models such as buoyant jets and wall jets in the BMIX++ code.

3. VALIDATION OF BMIX++

The BMIX++ code was successfully applied to various mixing problems such as stratification in a water tank due to a heater inside, water tank exchange flow experiment simulation, stratification produced by multiple plumes, and the UCB large containment mixing experiment which is composed of a rectangular enclosure with an isothermal cooling wall and a hot air jet injecting [10]. Most of these simulations gave satisfying results with small computation costs. These applications validated the BMIX++ code and showed its ability to analyze more complex mixing and heat transfer problems in large stably stratified enclosures. Due to page limits, here only one example is presented.

This section presents the application of the BMIX++ code to mixing experiments performed by Wong and Griffiths [22] in which two buoyancy sources produced well-separated, turbulent plumes. Figure 2 gives a schematic diagram of the general two-plume situation. One of interesting phenomena is that the source with the larger buoyancy flux produces a plume that descends to the bottom, while the source having a smaller buoyancy flux produces a plume that spreads at an intermediate depth. They also presented a numerical solution for the mixing process. The result by the BMIX++ simulation will be compared with the experimental data and the prediction by Wong and Griffiths.

The experiments released two dense salt solutions at a steady rate through two small nozzles protruding just below the free surface of a tank of water. Both the nozzles were 5×10^{-3} m in diameter. A peristaltic pump maintained a constant volume flux of salt water through the nozzles. Differences in buoyancy fluxes between the two sources were achieved by using salt solutions of different densities. The tank was 0.7 m long, 0.7 m wide and 0.5 m deep. The experiments were conducted with the nozzles placed on the centerline running along the length of the tank and 0.15 m from each end. The effective water depth was approximately 0.3 m. For the durations of the experiments in all cases, the total volumes of salt water added were insignificant compared to the volumes in the tank. All the experiments were started in homogenous tanks to study both the evolution and large-time behavior of the systems. The buoyancy flux is defined as

$$F = gQ_{in}\frac{\rho_i - \rho_a}{\rho_r}, \tag{39}$$

where Q_{in} is the volumetric flow rate of source, ρ_i the source inlet density, ρ_a the ambient density, ρ_r the reference ambient density, taken at the source inlet location. The split in buoyancy flux between the two sources is given by

$$\Phi = F_2 / F, \tag{40}$$

the ratio of the flux of the weak source to the total buoyancy flux. The first six experiments were carried out with the total buoyancy flux of $F = 8.97 \times 10^{-7}$ m^4/s^3, Φ ranged from 0.05 to 0.3, and $Q = 3.85 \times 10^{-7}$ m^3/s for each source. All six experiments ran for 30 min, the time required for the depth of the weak plume outflow to approach the final steady-state depth.

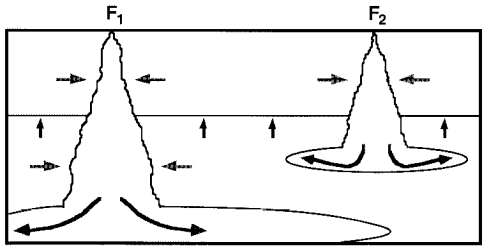

Figure 2 Schematic Diagram of the Two-Plume Filling-Box, F Is the Buoyancy Flux. (Courtesy of Wong and Griffiths [22])

Wong and Griffiths (W&G for later reference) extended Baines and Turner's method for a filling box [11] to calculate the mixing process with multiple plumes. Their solution includes one set of partial differential equation for the ambient and n sets of partial differential equation for each plume based on Morton's model [14]. They used a finite-difference scheme to solve the equations. Given an ambient density profile, each of the n sets of plume equations was solved separately using a fourth-order Runge-Kutta method. Then the ambient density profile was solved according to the solutions for plumes and the ambient governing equations. The new profile was then used to calculate the plume properties and the cycle repeats. W&G's method is quite similar to the methods of the BMIX++ code, except that the BMIX++ code uses much more general ideas to calculate the mixing processes (entrainment and discharge, two-tiers scaling) and uses the Lagrangian method instead of traditional finite-difference method to solve ambient equations. We can say that W&G's method is a special example of the methods used by the BMIX++ code. Therefore, comparison with the experiments and W&G's predictions provides an interesting validation case for the BMIX++ code.

W&G used nondimensional properties to express their experimental and numerical results. The followings are some of such nondimensional properties:

$$\zeta = z / H, \tag{41}$$

$$\tau = t / \left(2^{-4/3} A \cdot E^{-4/3} \pi^{-2/3} H^{-2/3} F^{-1}\right), \tag{42}$$

$$f_e = g \frac{\rho_a - \rho_r}{\rho_r} \Big/ \left(2^{-4/3} E^{-4/3} \pi^{-2/3} H^{-5/3} F^{2/3}\right), \tag{43}$$

where H is the effective height of the buoyancy sources, A the cross section area of the enclosure, E the entrainment coefficient taken as 0.129, and, F the total buoyancy flux.

In the BMIX++ simulation, Morton's analytical model was used to calculate the strong plume, and Schatzmann's model was used to calculate the weak plume. A time step of 5 seconds was used in the simulations. How to calculate the discharge location is a complex problem. The actual discharge process for a plume happens not at a point but instead in a region. Firstly, the outer part of the plume will spread into the ambient fluid, and then the inner core will finally become a part of the ambient. W&G used the neutral buoyancy level as the discharge level where the plume density average equal to the density of the ambient fluid. In reality, the neutral buoyancy level underestimates the actual discharge because the momentum of the plume at the neutral buoyancy level is not zero and both of velocity and density distributions in the plume is not homogenous. Schatzmann's model uses an entrainment model depending on the local densimetric Froude number. The first term in the RHS of Eq. 26 is for momentum effect, and the second term is for buoyancy effect. From this entrainment model, an easy method to specify the start point of discharge is to check where the entrainment coefficient changes to negative sign. Figure 3 shows the discharge depths of the weak plume for W&G's model and for the BMIX++, and, the depth of the lower extent of the weak plume intrusion. From the figure, the discharge levels used by W&G's model and by the BMIX++ code are close. Both of discharge levels decrease with the increase of the buoyancy flux of the weak plume.

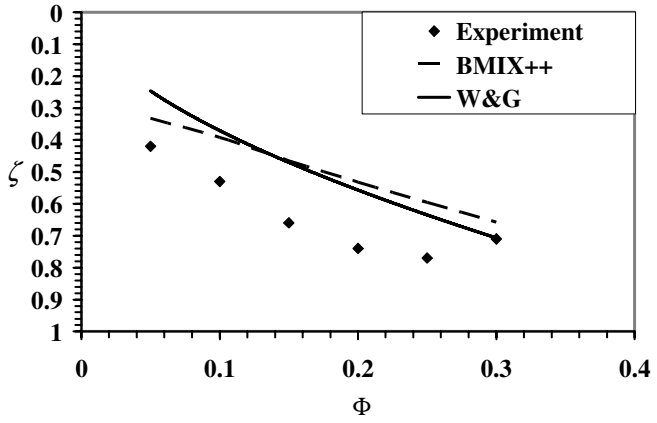

Figure 3 the Discharge Depth of the Weak Plume in W&G's Model and in the BMIX++ Simulation, and, the Depth of the Lower Extent of the Weak Plume Intrusion from W&G's Experiment, ζ Is the Non-dimensional Depth and Φ the Ratio of the Flux of the Weak Source to the Total Buoyancy Flux.

Figure 4 shows the first front variation with time for the case of Φ=0.1. The BMIX++ predicts very well for the first front, although the prediction is a little higher than the prediction by W&G and experiment. There are two reasons. The first reason is that Schatzmann's entrainment model is a generic model for a buoyant jet, and no data fitting technique was used to select a model constant for a special case; while W&G determined the entrainment constant *E* by comparing the progress of the first front in single-plume experiments with Baines and Turner's theoretical solution for the first front. Another reason is that the input data for the BMIX++ simulation were extracted from W&G's paper. Some data were approximately expressed, such as the effective height. Figure 5 shows several nondimensional environmental density profiles at different time instances for the case Φ=0.1. The predictions by the BMIX++ code and by the W&G are very close and agree very well with the experiment, especially for the long-term profiles. It seems that

the BMIX++ gave a little better prediction for the long-term profile than W&G's model. For the short term, both numerical model predicted unreal sharp density variation near discharge levels due to imperfect discharge models.

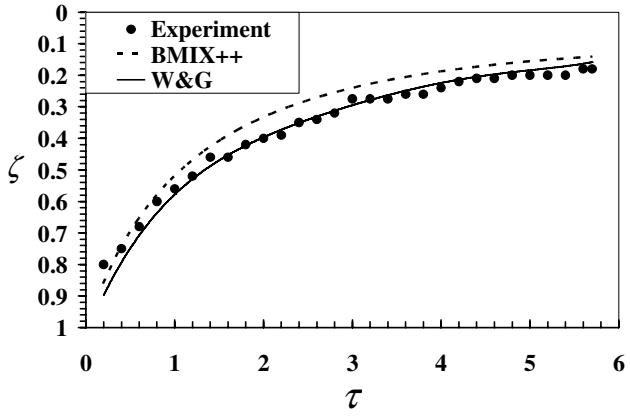

Figure 4 the Positions of the First Front for Φ = 0.1, ζ Is the Non-dimensional Depth, τ the Non-dimensional Time, and Φ the Ratio of the Flux of the Weak Source to the Total Buoyancy Flux.

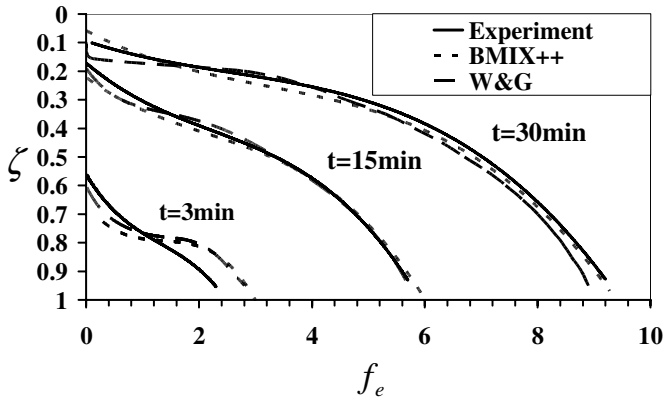

Figure 5 the Environment Buoyancy Profiles f_e for Φ = 0.1, ζ Is the Non-dimensional Depth and Φ the Ratio of the Flux of the Weak Source to the Total Buoyancy Flux.

In summary, the application of the BMIX++ code to the mixing due to multiple plumes shows the ability of this code in more complex configurations. Note that the BMIX++ code is a general code for the mixing and heat transfer in large enclosures with a stratified ambient. It is very easy to construct an input file for different configurations. Different models for jets and plumes can be chosen and combined. These features make the BMIX++ code superior to those specific methods such as W&G's method.

4. AHTR BUFFER POOL THERMAL STRATIFICATION ANALYSIS

This section describes AHTR buffer pool thermal stratification problems and presents the simulation results. Fig. 6 and 7 show the elevation and plan views of AHTR-MI design [2]. AHTR-MI design is a hybrid of loop and pool designs. The primary loop including reactor

vessel, IHX, pumps, and connecting pipes, is immersed in buffer salt (NaF-NaBF4) which has lower melting point than primary salt (flibe). Heat removal from the buffer salt to the environment occurs dominantly through DHX. The primary system and the buffer salt tank system are thermally coupled by the PRACS, which is composed of PHX, fluidic diodes and connecting pipes. A fluidic diode reduces leakage flows under primary loop forced circulation. Fluidic diodes are simple, passive devices that provide large flow resistance in one direction. The simplest fluidic diode devices generate an irreversible loss of kinetic energy by creating a strong vortex flow in one direction, while flow in the opposite direction does not have this effect. Both DHX and PHX modules are in baffles to enhance natural circulation as shown in Fig. 6.

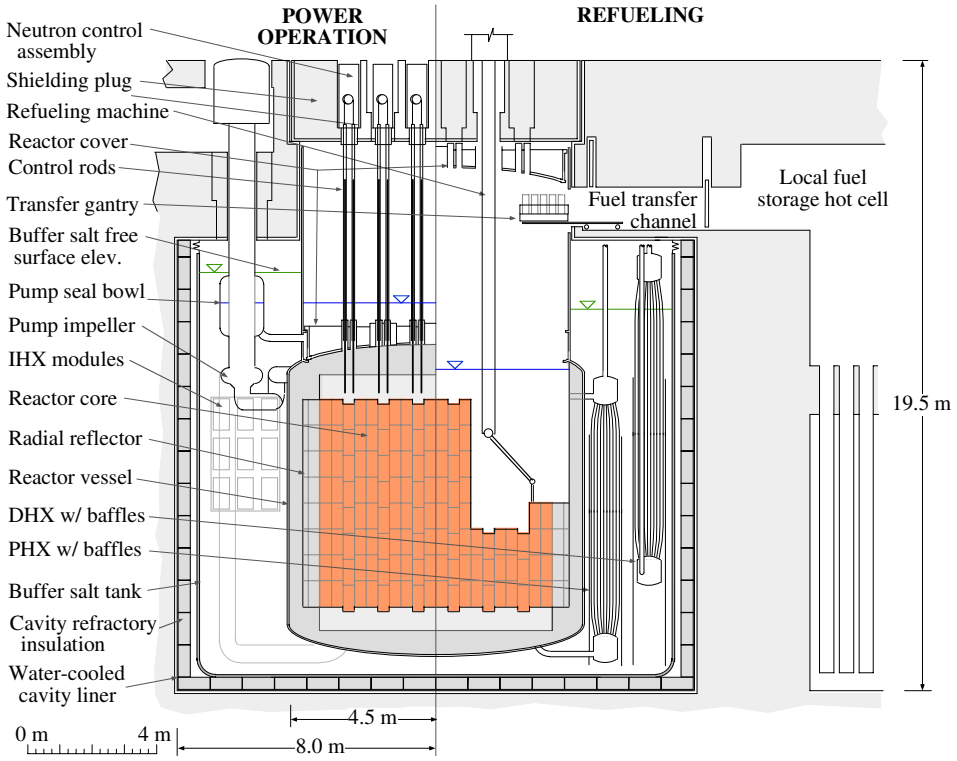

Figure 6 Elevation View of the AHTR-MI, for Normal Operation (Left) and Refueling (Right) Modes.

For normal power operation with forced cooling, the primary loop operates in forced circulation, transferring heat to four intermediate liquid salt loops using modular, compact IHX located in the buffer salt tank. Upstream of the IHX modules are the four primary pumps, which take suction from the core outlet plenum at near atmospheric pressure. A small bypass with reactor inlet temperature flows upward through PHX. This bypass flow heats the buffer salt. This added heat is mainly removed by the DHX so that the buffer salt temperature remains constant. A RELAP5/3D simulation [23, 24] shows that the bypass flow through PHX is about 1% of the total flow rate. According to this result, the heat transfer rate through the PHX, the buffer salt side temperature change and the mass flow rate through the PHX can be calculated using the lumped-volume method by solving momentum and energy conservation equations. Similarly, the buffer salt side temperature change and mass flow rate through the DHX buffer salt side can be obtained.

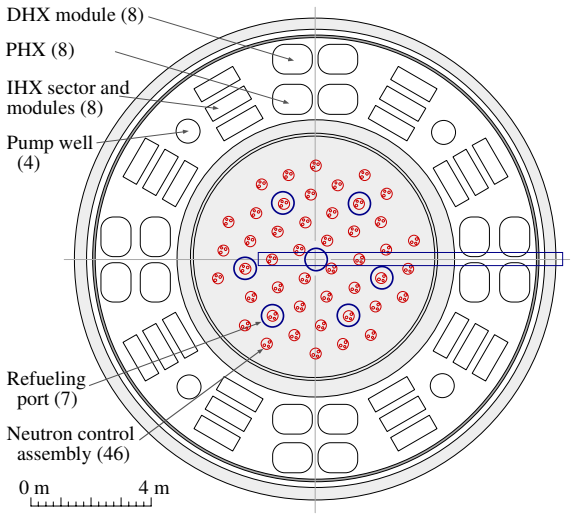

Figure 7 Plan View of the AHTR-MI.

Under the loss of forced primary loop circulation (LOFC) transient with reactor scram, reduced heat transfer in the reactor core causes the core temperatures to rise. Natural circulation establishes quickly and flow reversal happens through PRACS loops. Due to higher flow resistance in IHX and usually loss of secondary heat sink, natural circulation through IHX is not important for decay heat removal compared to heat removal by the PRACS. Decay heat removal then occurs through the 8 PHX modules. The PHX heat transfer area is sized to match decay heat generation approximately 1 to 2 hours after loss of LOFC occurs. The DRACS heat removal systems are sized to match decay heat generation approximately 12 to 48 hours after LOFC occurs.

Both the PRACS and DRACS system designs have not been optimized. PHX modules can extend full core height or use only part of that while keep same heat transfer area. Analysis shows the later case can increase natural circulation. Therefore the case with half core height is considered in this stratification study. Another design option is how to arrange baffles around heat exchanger modules to enhance natural circulation and reduce thermal stratification. In Fig. 6, the baffle around DHX modules is extended to near the bottom of the pool. This paper includes three cases to compare baffle arrangement effects on thermal stratification: case 1 with no extended baffles beyond heat transfer sections; case 2 with no extended baffle for the PHX but with an extended baffle for the DHX; and case 3 with extended baffles for both the PHX and DHX. Figure 8 shows the simplified major driving mechanism for thermal stratification. Heat losses through reactor vessel, IHX, pipes, and buffer salt tanks are ignored. Because PHX and DHX modules are enveloped with baffles to enhance natural circulation, for PHX, ambient buffer salt enters the bottom of PHX modules as mass sinks (relative to ambient fluid) and warmer buffer salt rises from the top of PHX modules as buoyant jets; for DHX, ambient cold buffer salt enters the top of DHX modules as mass sinks and colder salt flows downward from the bottom of DHX modules as buoyant jets. In the simulation, 8 upward buoyant jets from the PHX modules and 8 downward buoyant jets from DHX modules are simulated. The inlets for PHX and DHX modules are simulated as mass sinks.

The precise inlet/outlet temperatures from the baffles around the PHX and DHX can only be calculated by coupling a system analysis code and thermal mixing code like BMIX++. However, this coupling has not yet been realized. For steady calculations, we can use iterative methods to approximate this problem. First, the buffer salt pool is assumed to have uniform temperature and the PHX and DHX outlet temperatures in the buffer salt side are then estimated because we already know the temperature difference between the inlet and outlet. Then the new steady temperature profile in the buffer pool is calculated by BMIX++ code and this information is used to set the new PHX and DHX inlet temperatures and calculate new outlet temperatures. Several iterations generate a converged result.

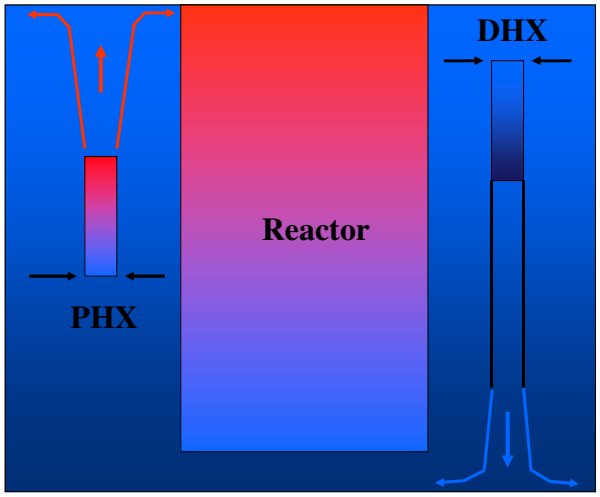

Figure 8 Schematics of Major Driving Forces for Thermal Stratification in Buffer Salt Tank.

For the LOFC transient, accurate buoyant jet information such as outlet temperature and volumetric flow rate can only be obtained using a coupled calculation between a system analysis code and a mixing code. One simplified method for transient thermal stratification analysis is to assume that heat transfer rate through the PHX remains constant at about 1% of normal power in the first few hours of the LOFC transient. This assumption can be supported by observing the transient response of AHTR-MI in a typical LOFC transient [2]. For cold jets from the DHX, steady state parameters are assumed. This assumption is not strictly valid and is made only as a zero order simplification to show general transient behavior of the buffer salt pool.

Table I summarizes the major simulation parameters for substructures including upward buoyant jets, downward buoyant jets, and two mass sinks for different cases. To simplify the simulation, the mass sinks for the 8 PHX modules are treated as one sink and the mass sinks for the 8 DHX modules are treat as one sink. The buffer salt tank is assumed to have constant cross-sectional area of 111.2 m^2 and a total height of 12.8 m. The normal average temperature in the buffer salt is 500°C. The PHX and DHX baffle diameters are 0.883 m. The PHX modules are located from 5.2 m to 8.4 m elevations (all the elevations are relative to the bottom of the buffer salt tank) and the DHX modules are located from 7.8 m to 11 m. LOFC thermal stratification analysis is only done for case 1.

Figure 9 shows the temperature profile in the buffer salt pool for the case 1 configuration, as calculated by the BMIX++ code. Due to the competing effects by one group of upward hot buoyant jets, one group of downward cold buoyant jets, and two groups of mass sinks, there are two thermal fronts: the upper one for the hot jets and the lower one for the cold jets. Thermal stratification in buffer salt is divided into three regions: the top region above the PHX, the lower region below the DHX, and the middle one between the PHX and DHX. The temperature difference between the top and bottom for normal operation is about 7.7°C. Figure 9 shows that under LOFC transient conditions the PHX heating power increases and the driving force for thermal stratification becomes stronger. Therefore the thermal stratification in the buffer salt becomes larger (12.7°C at the time of one hour). Larger thermal stratification can be expected in the later stage of a LOFC transient and more severe transients such as LOFC without scram. From Fig. 9 we can see that the thermal front profiles are predicted to be very sharp. These high temperature gradients may cause higher local thermal stresses in the buffer salt tank wall and other structure materials.

Table I. Major input parameters for substructures

Case Number	Substructures	Locations, m	Temperature, °C	Source volumetric flow rate, m^3/s
1	PHX jets at steady state	8.4	504.8	0.0544
	PHX mass sink at steady state	5.2	set by ambient fluid	0.4352
	DHX jets	7.8	497.1	0.0544
	DHX mass sink	11	set by ambient fluid	0.4352
	PHX jets in LOFC at hour one	8.4	510.2	0.0741
	PHX mass sink in LOFC at hour one	11	set by ambient fluid	0.5928
2	PHX jets	8.4	504.3	0.0544
	PHX mass sink	5.2	set by ambient fluid	0.4352
	DHX jets	0.5	496.6	0.0544
	DHX mass sink	11	set by ambient fluid	0.4352
3	PHX jets	8.4	528.6	0.0136
	PHX mass sink	0.5	set by ambient fluid	0.1088
	DHX jets	0.5	497.8	0.0544
	DHX mass sink	11	set by ambient fluid	0.4352

Fig. 10 shows the temperature profile in the buffer salt pool for the case 2 configuration. In this case, the baffle around the DHX is extended to near the pool bottom. This cold section has the effect of a chimney to enhance natural circulation through PHX and is therefore favorable. The

pool thermal stratification for this case is quite similar as case 1. The pool has three zones with different temperatures. The top zone temperature and the lower zone temperature are both slightly lower than the corresponding values for case 1. But the middle zone volume for case 2 is much larger than for the case 1.

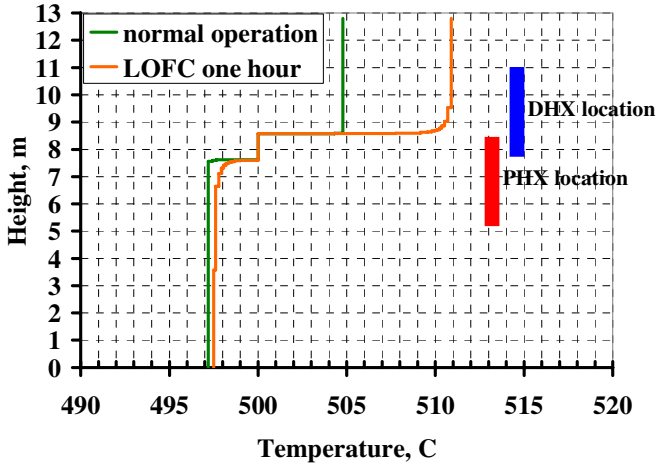

Figure 9 Temperature Profiles in Buffer Salt Tank for Steady State operation, and for LOFC at One Hour for Case 1.

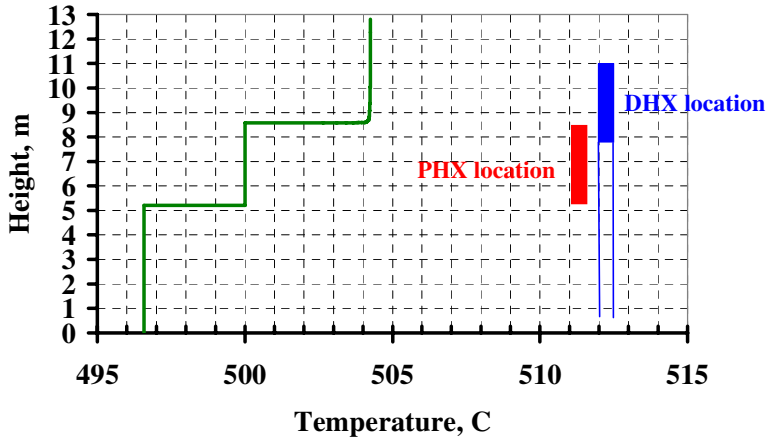

Figure 10 Steady State Temperature Profile in Buffer Salt Tank for Case 2.

Fig. 11 shows the temperature profile in the buffer salt pool for case 3. Both baffles around the DHX and PHX are extended to near the pool bottom. At a first examination, this arrangement may let the PHX draws cold salt into it and reduce the outlet temperature. However, cold salt fills in the extended baffle below the PHX modules, which greatly reduces the available buoyancy force that drives the natural circulation through heat transfer sections. Therefore, flow rate through PHX significantly decreases through PHX and outlet temperature increases notably in order to remove same amount of heat. The resulting thermal stratification as shown in Fig. 11 is much larger (16.3ºC) than the first two cases (7.7ºC). Therefore, case 3 should not be used in design. Among the three arrangements, the baffle configuration in case 2 provides the best

choice. Although highly simplified, the analysis given above already shows the potential of BMIX++ code in optimization of pool system design.

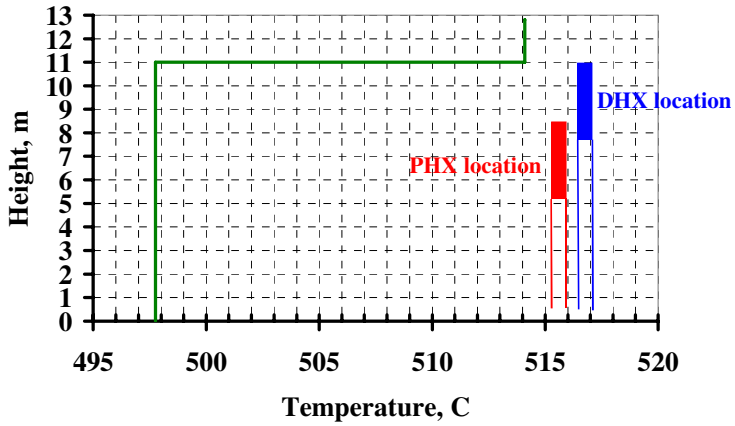

Figure 11 Steady State Temperature Profile in Buffer Salt Tank for Case 3.

5. CONCLUSIONS

Unlike traditional LWR reactors, Gen. IV pool type reactor concepts such as AHTR and SFR typically have very large thermal inertia and no active engineered safety systems that would provide a strong momentum source to generate mixing. Therefore, transient and accident processes tend to be mild and slow, allowing buoyancy forces to dominate the system. Thermal stratification often appears in such enclosure or tank systems. Traditional system analysis codes are developed for loop systems with strong momentum or mass sources, where control volumes can be assumed to be well mixed with relatively low error. These codes have no ability to calculate complex thermal stratification and mixing problem. Scaling based one-dimensional methods such as BMIX++ used can give satisfying results without resorting to expensive CFD simulation, therefore are well suited to couple with system analysis codes for Gen IV reactors such as the SFR and AHTR, and advanced LWRs. The AHTR buffer pool thermal stratification analysis demonstrates the ability of BMIX++ code to simulate complex thermal stratification and mixing problems and help to optimize the pool system design and baffle configuration. Similar analysis is possible for liquid-metal cooled reactors.

ACKNOWLEDGMENTS

This work was supported through the INL Laboratory Directed Research and Development Program under DOE Idaho Operations Office Contract DE-AC07-05ID14517. BMIX++ code development work was mainly supported through DOE NEER award to UCB under the Contract DE-FG07-99ID13769.

NOMENCLATURE

A area, [m^2]
b jet width parameter, [m]

B	buoyancy flux, [m^4/s^3]
c_i	mass fraction of species for i component, [-]
c_p	specific heat capacity, [J/kg-K]
D	mass diffusivity, [m^2/s], or diameter, [m]
E	entrainment, [m^2/s]
f_e	the non-dimensional environment buoyancy, [-]
F	vector of fluxes, or buoyancy flux, [m^4/s^3]
Fr	local densimetric Froude number, [-]
g	gravitational acceleration, [m/s^2]
g'	reduced gravity, [m/s^2]
G	vector of conserved quantities
h	enthalpy, [J/kg]
$\bar{h}$	volume averaged enthalpy, [J/kg]
H	height, [m]
k	thermal conductivity, [W/m-K]
k_μ	Taylor's entrainment constant, [-]
P	pressure, [Pa]
$\dot{q}$	heating rate, [W]
q''	heat transfer rate, [W/m^2]
Q	volume flow rate, [m^3/s]
Q'	entrainment rate, [m^2/s]
r	radial coordinate, [m]
R	radius, [m]
s	coordinate along jet trajectory, [m]
S	vector of sources, or volume source, [m^3/s]
$\hat{S}$	volume sink, [m^3/s]
S'	volumetric source per unit length, [m^2/s]
$\hat{S}'$	volumetric sink per unit length, [m^2/s]
S_h	source of energy per unit time [W]
$\hat{S}_h$	sink of energy per unit time [W]
S_h'	volumetric energy source per unit length, [W/m^2]
$\hat{S}_h'$	volumetric sink per unit length, [W/m^2]
t	time, [s]
Δt	time step length, [s]
T	temperature, [K]
u	velocity, [m/s]
U	jet centerline velocity, [m/s]
v_r	radial velocity, [m/s]
V	volume, [m^3]
$\dot{V}''$	volumetric flow rate per unit area, [$m^3/(m^2$-s)]
x	cross direction coordinate, [m]
z	vertical direction coordinate, [m]

Greek symbols:

α	the entrainment constant, [-]
β	volumetric thermal expansion coefficient, [K^{-1}] or a coefficient in entrainment models, [-]
ε	dimensionless entrainment coefficient, [-]
ζ	non-dimensional depth, [-]
θ	angle with the horizontal direction, [rad]
λ	spreading ratio of mass and heat versus momentum, [-]
ρ	density, [kg/m^3]
$\overline{\rho}$	volume averaged total density, [kg/m^3]
τ	nondimensional time, [-]
Φ	the ratio of the flux of the weak source to the total buoyancy flux, [-]
χ	mass fraction, [-]
$\overline{\chi}$	volume averaged mass fraction, [-]

Subscripts:

0	source or reference
a	ambient
amb	ambient
i	index for species
in	inlet
j	index for jet source
k	index of control volume
l	buoyant jet index
mix	mixture
n	number of jets
ns	number of species
p	plume
r	reference
s	source
sf	ambient, stratified fluid
v	virtual source
∞	ambient

Superscripts:

*	plume or jet excess value on the centerline
j	index for time level

ACRONYMS

AHTR	Advanced High Temperature Reactor
BMIX++	Berkeley mechanistic MIXing code in C++
CFL	Courant-Friedrichs-Levy stability criterion

CV	Control Volume
DHX	DRACS Heat eXchanger
DRACS	Direct Reactor Auxiliary Cooling System
IHX	Intermediate Heat eXchanger
LOFC	Loss Of Forced primary loop Circulation
PHX	PRACS Heat eXchanger
PRACS	Pool Reactor Auxiliary Cooling System
RK	Runge-Kutta method
RKF	Runge-Kutta-Fehlberg method
SFR	Sodium Fast Reactor

REFERENCES

1. C.W. Forsberg, P. Pickard, and P.F. Peterson, "Molten-Salt-Cooled Advanced High-Temperature Reactor for Production of Hydrogen and Electricity," *Nuclear Technology*, **Vol. 144**, pp. 289-302 (2003).
2. P.F. Peterson and H. Zhao, **"**A Flexible Base-Line Design for the Advanced High-Temperature Reactor Utilizing Metallic Reactor Internals (AHTR-MI)," *Proceedings of the 2006 International Congress on Advances in Nuclear Power Plants, ICAPP'06*, Reno, NV, USA, June 4-6, pp. 650-661 (2006).
3. S. Moriya, N. Tanaka, N. Katano and A. Wada, "Effects of Reynolds number and Richardson number on thermal stratification in hot plenum," *Nuclear Engineering and Design*, **Vol. 99**, pp. 441-451 (1987).
4. INL, "RELAP5-3D Code Manual," *INEEL-EXT-98-00834, Rev. 2.4,* June (2005).
5. J.W. Spore, et al., "TRAC-M/FORTRAN 90 (Version 3.0) Theory Manual," *LA-UR-00-910*, July (2000).
6. P.J. Finck, "Fast Reactor Simulation Challenges," *DOE National Laboratory Workshop Advanced Simulations: A Critical Tool for Future Nuclear Fuel Cycles,* LLNL, Livermore, California, December 14 (2005).
7. P.F. Peterson, "Scaling and Analysis of Mixing in Large, Stratified Volumes," *International Journal of Heat and Mass Transfer*, **Vol. 37, Suppl. 1,** pp. 97-106 (1994).
8. J. Christensen and P.F. Peterson, "A One-Dimensional Lagrangian Model for Large-Volume Mixing," *Nuclear Engineering and Design*, **Vol. 204**, pp. 299-320 (2001).
9. H. Zhao, *Computation of Mixing in Large Stably Stratified Enclosures*, Ph.D. dissertation, University of California, Berkeley (2003).
10. F. Niu, H. Zhao, P.F. Peterson, J. Woodcock, and, R.E. Henry, "Investigation of Mixed Convection in a Large Rectangular Enclosure," *Nuclear Engineering and Design*, **Vol. 237**, pp. 1025–1032 (2007).
11. W.D. Baines, and J.S. Turner, "Turbulent Buoyant Convection from a Source in a Confined Region", *Journal of Fluid mechanics*, **Vol. 37**, pp. 51-80 (1969).
12. R.J. Fox, D.B. McDonald, P.F. Peterson, and V.E. Schrock, "Temperature Distribution in Pools with Shallow Buoyant Jets," *Proceeding of Fifth International Topical Meeting on Nuclear Reactor Thermal Hydraulics (NURETH-5)*, Salt Lake City, Utah, USA, September, 21-24, Vol. 4. pp. 1227-1234 (1992).

13. M. Gavrilas, N.E. Todreas and M.J. Driscoll, “The design and evaluation of a passively cooled containment for a high-rating pressurized water reactor,” *Nuclear Engineering and Design*, **Vol. 200, Issues 1-2,** pp. 233-249 (2000).
14. B.R. Morton, "Forced Plumes," *Journal of Fluid mechanics*, **Vol. 5**, pp. 151-163 (1959).
15. M. Schatzmann, “The Integral Equations for Round Buoyant Jets in Stratified Flows,” *J. Appl. Math, Phys. (ZAMP)*, **Vol. 29**, pp. 608-630 (1978).
16. M. Schatzmann, “A Integral Model for Plume Rise,” *Atmos. Environ.*, **Vol. 13**, pp. 721-731, (1979).
17. G.A. Davidson, "A Discussion of Schatzmann's Integral Plume Model from a Control Volume Viewpoint," *Journal of Climate and Applied Meteorology*, **Vol. 25**, pp. 858-867, (1986).
18. M.A.C. Teixeira, and P.M.A. Miranda, “On the Entrainment Assumption in Schatzmann’s Integral Plume Model,” *Applied Scientific Research*, **Vol. 57**, pp. 15-42, (1997).
19. G.F. Lane-Serff, P.F. Linden, and M. Hillel, "Forced, Angled Plumes," *Journal of Hazardous Materials*, **Vol. 33**, pp. 75-99, (1993).
20. T. Log, and G. Heskestad, "Temperatures of Restricted Turbulent Fire Plumes," *Fire safety Journal*, **Vol. 31**, pp. 101-115, (1998).
21. G. Hall and J.M. Watt, *Modern Numerical Methods for Ordinary Differential Equations*, Clarendon Press, Oxford, UK (1976).
22. A.B.D. Wong and R.W. Griffiths, “Stratification and Convection Produced by Multiple Turbulent Plumes,” *Dynamics of Atmospheres and Oceans*, **Vol. 30**, pp. 101–123, (1999).
23. A. Griveau, F. Fardin, H. Zhao, and P.F. Peterson, “Transient Thermal Response of the AHTR-MI to Loss of Forced Cooling,” *Proceeding of GLOBAL 2007, Advanced Nuclear Fuel Cycles and Systems*, Boise, Idaho, USA, September 9-13, (2007).
24. A. Griveau, “Modeling and Transient Analysis for the Pebble Bed Advanced High Temperature Reactor (PB-AHTR),” UCBTH-07-001, MS Thesis, University of California, Berkeley, Feb, (2007).